Direct numerical simulations of flutter instabilities over a vibrating turbine blade cascade

M. E. Nakhchi[1], M. Rahmati

Department of Mechanical and Construction Engineering, Northumbria University, Newcastle upon Tyne NE1 8ST, UK

Abstract

This paper presents direct numerical simulations (DNS) on unsteady turbulent flow in a vibrating low-pressure turbine blade cascade to predict the flutter instabilities and explores the effects of blade oscillations on the flow structure and flow separation point. The spectral/hp element method is employed for the three-dimensional simulations of the domain. This method enables capturing more details about the flow structure and vortex generations compared to the URANS methods. The method can aid in understanding the physics of these complex fluid structure interaction problems while it requires much less computational time compared to the other DNS models. The blade vibration frequency is varied from 5.2Hz to 10.3Hz with maximum vibration amplitude of 3% of chord length at the blade tip. The results illustrate that the vortex generation becomes stronger over the blades with higher vibration frequencies compared to the stationary ones. The main reason for the additional vortex generation and recirculations over the oscillating blades is the additional flow disturbance due to blade vibration and its interactions with the shear-layer on the turbine blade cascade. It is seen that the vortex shedding is growing around the trailing edge and become stronger on the suction surface of the vibrating blade. The flow separation over the suction surface of the stationary blade occurs at S_{sep}/S_0=0.391, while it occurs at 0.372 over the oscillating blade with f=5.2 Hz.

[1] Corresponding author (mahdi.nakhchi@northumbria.ac.uk)

Keywords: Direct numerical simulations; Pressure turbine; Blade oscillations; Turbulent flow; Fluid-structure interaction.

Nomenclature

Symbols		**Greek symbols**	
A	Vibration amplitude	α	Angle of attack
C	Chord	θ	momentum thickness
C_p	Pressure coefficient	ν	Kinematic viscosity
f	Vibration frequency	ω	Vibration frequency
L	Blade span	Ω	Computational domain
P	Pressure	**Subscripts**	
P	Polynomial order	in	inlet
Q	Fourier coefficient	ref	Reference
Re	Reynolds number	sep	Separation point
S	Blade suction surface		
u	Velocity vector		
w_z	Spanwise vorticity		

1. Introduction

The motion of adjacent blade rows in turbomachinery produces unsteady fluid flow motions, which could have an undesirable effect such as noise propagation and flutter instabilities [1]. In modern turbine blades, those effects are intensified as they are typically designed with high loadings and more compact structures. One important characteristic of modern Low Pressure Turbines (LPTs) is their complex transient and flow separation regimes. This transient flow may interact with blade's structural movement in complex non-linear fashion. So, there are increasing needs to accurately predict this complex fluid structure interaction (FSI) problem, which can lead to flutter instabilities, especially for low pressure turbines with long blades.

Many researchers performed numerical simulations to predict the flutter instability and forced response in turbine blade cascade in the past years. An efficient method proposed by Giles [2] is time-linearized nonlinear harmonic technique. This technique divides the transient flow equations into the single time-averaged equation and single time-linearized equation. The

transient flow perturbations are depicted in the Fourier series. These common harmonic techniques utilizing a pseudo-time-marching method usually represent solution divergence behavior for separation fields. To resolve this challenge new frequency domain methods such as phase-solution method [3] and harmonic-balance method [4] have been developed and utilized for turbomachinery aeromechanic applications in recent decades. These methods solve transient governing equations with a particular alternative unsteadiness at 3 specific phases of a period of instability and get similar computation effectiveness as a typical time linearized technique. Some recent studies focused on wake control and investigated the impact of the geometry structure on the wake profile [5, 6]. It was found that controlling wake structure can reduce the transient forces and oscillations in marine structures.

Precise estimation of flutter and forced response in turbomachinery is one of the biggest unresolved challenges faced by the industry [7]. Significant efforts have been made over the last decade to get effective numerical approaches for aeromechanical analysis [8]. Those methods have been developed for industrial design and may not be adequate for simulating flow over advanced LPTs where flow separation will occur. So, developing more accurate high fidelity numerical models is essential for understanding complex flow in a modern LPT turbine under vibration. In the numerical study of Rahmati et al. [9], nonlinear frequency-domain technique was employed to predict the pressure coefficient and aero-damping of multistage turbine blades. The results were compared with the time domain method and good agreement was observed. Shine et al. [10, 11] conducted numerical investigations on aeroelasticity analysis of wind turbine blades. Their results revealed that the frequency-domain method could predict the unsteady pressure distribution and aero-damping on the wind turbine blades with significantly lower computational time compared to URANS methods. In industry, these low fidelity methods are highly desirable as the focus is on the value of aero-damping and the complex physics occurring during fluid-structure interactions are disregarded. This, however,

gives rise to a black-box effect, which leaves physical understanding behind. Therefore, a higher fidelity numerical model is essential to further explore the flow physics concerning these coupled effects and subsequently inform the low-fidelity models. This is particularly important for modern aeronautical low-pressure turbines which are made of very slender and thin air-foils and as a result flutter may become a dominant constraint on the design of them. Vahdati and Zhao [12] used URANS to numerically predict the effects of different intakes on the fan blade flutter instability. They concluded that stall and acoustic flutter could be observed on the blade surface. Their computational fluid dynamics (CFD) simulations showed the details of the mechanism for acoustic flutter as a result of the unsteady pressure waves. Peters et al. [13] performed numerical fluid-structure interaction (FSI) simulations to investigate the aerodynamic damping of a vibrating fan blade. They concluded that the formation of the vortex shedding near the leading edge of the blade depends on the blade's angle of attack. In the review study of Rashidi et al. [14], it was concluded that the vortex shedding near the aerodynamic bodies can be controlled by using different active and passive methods, resulting in fewer structure oscillations. In order to solve the momentum equations of incompressible Navier-Stokes flow, a pressure field is required. However, no obvious equation exists for obtaining the pressure field. In dealing with this difficulty, one approach uses the vortex method where the pressure parameter was eliminated from the momentum equations by solving the vorticity transport equations. Various other methods such as the artificial compressibility method [15, 16] mentioned, exist. In the artificial compressibility technique, the continuity equation is changed to contain an artificial compressibility term that disappears when a steady state is achieved. Another method which is pressure correction method. In the pressure correction methods, the momentum equation is resolved in the beginning with an adopted pressure field that is updated by iterations utilizing a pressure correction equation. Applications of these methods to turbomachinery flow have been carried out by Lakshminarayana [17] and

Rhie and Chow [18], among many others. In comparison to the artificial compressibility method, pressure correction methods are more widely used in turbomachinery applications. These methods have lower storage requirement than artificial compressibility methods."

Higher accuracy CFD methods such as Large-Eddy Simulations (LES) or Direct Numerical Simulations (DNS) can provide a detailed view of the physical behavior of the transient turbulent flows. Wang et al. [19] employed LES to capture the flow separating point and recirculations over an LPT blade cascade. It was observed that LES is more accurate compared to the other turbulent RANS models. Zhe et al. [20] developed a new numerical method to evaluate the aeroelastic wake behavior of the turbine blades. The air inflow velocity was between 8 to 11.4 m/s in their study. The aerodynamic coefficients and other important parameters such as power and natural frequencies of the oscillating blades were compared with the literature to show the accuracy of the proposed model. The velocity distribution in the wake region of the turbine blades was also investigated by the authors. To et al. [21] numerically investigated the effects of vibrations and deformed trailing edge of an airfoil in transonic regime at high Reynolds numbers. The Reynolds number was 2.06×106, and the Mach number of 0.76 was used in their study. The Navier–Stokes MultiBlock solver, including adapted turbulence model was employed to capture the flow structure over the airfoil blade. The vibration frequency was between 200Hz to 500Hz in their numerical simulations. It was observed that the vibration frequency has significant effect on the flow structure and vortex shedding near the edge of the airfoil. Apsley and Stansby [22] numerically investigated the transient thrust on oscillating wind turbines. They observed that the oscillations have a considerable effect on the load coefficient over the blades. In the CFD analysis of Rashidi et al. [23], the vortex shedding and flow behaviour over a circular obstacle were investigated numerically. They used SIMPLE algorithm to perform the simulations at the Reynolds number of 100. They found that using a magnetic field can control the flow separation and vortex

shedding over the surface of the obstacle. The effects of the proposed magnetic field were also investigated on the drag and lift coefficient.

Tucker [24, 25] showed that unsteady Reynolds average Navier-Stokes (URANS) models are not accurate enough to capture the details of the flow separation point and the recirculating flows in the separated region on the surface of the turbine blades. Muller et al. [26] conduced DNS over a low-pressure turbine blade under turbulent flow regime. The results were compared with the URANS model, and it was observed that the DNS is more accurate, but it requires a huge amount of computation time. The direct numerical simulations of Zarki et al. [27] inside linear compressor cascades showed that the incoming wakes cause the boundary-layer disruptions over the blade. In another numerical study, Wheeler et al. [28] used DNS to investigate the flow structure and the details of the boundary layer in a high pressure turbine cascade. They also captured the time-average vorticity contours in the span direction at different phases. The location of the flow separation point was found to have weak phase-dependency. The DNS methods have been developed in recent years for different fluid dynamics applications [29, 30], but the main disadvantage of the current DNS models is the huge amount of the required computation units which reduces the efficiency of the computations. Therefore, developing a DNS methodology with reduced amount of computation unit requirement can significantly improve the efficiency of the computations together with achieving higher accuracies.

Spectral/hp element approach is a new and very accurate DNS technique that contains the benefits of lower-order finite element methods together with spectral element techniques. By employing this technique, the computational time could be considerably reduced while the accuracy remains high and even be improved by increasing the polynomial order compared to the other DNS methods. This technique was firstly developed by Karniadakis and Sherwin [31] to simulate incompressible turbulent flow aerodynamics. They concluded that that this highly

accurate spectral/hp element method can be used in both compressible and incompressible fluid dynamics with reduced CPU time requirements. This method can additionally be utilized to capture the unsteady flow structures and perturbations in transitional flow regimes at different Reynolds numbers [32]. This technique is now available in open-source code named NEKTAR++. In the numerical study of Bao et al. [33], spectral/hp element approach was utilized to capture the unsteady stream fluctuations and vortex generation on an oscillating cable. The simulations were performed at Reynolds number of 3900 with 16 strips in the span direction. They remarked that the vibrations can considerably alter the flow structure over the cable structure. Bao et al. [34] developed the fluid/structure interaction ability of the spectral/hp element technique to evaluate the drag and lift coefficients over a three-dimensional flexible riser. It was concluded that the obtained DNS data are in agreement with the experimental results.

The above literature review shows that a few DNS methods have been used to resolve the unsteady flow in turbomachines. However, there is no DNS study to precisely simulate the transient flow structures on the turbine cascade by considering blade vibrations and under realistic turbulent flow conditions. In this study, a highly efficient DNS model depending on the spectral/hp element technique is used for analysing turbulent flows over an oscillating blade and the details of unsteady pressure are compared with experimental data for the first time. Accurate prediction of the flow structure and analysing the effects of blade oscillations with different frequencies on the flow separation and boundary-layer flow over the blades can help designers to improve the performance of the rotor blades at high flow speeds. The focus of the paper is on the DNS for Aeroelasticity over the vibrating turbine blade by using the developed NEKTAR++ code. The incompressible Navier-Stokes equations over the vibrating turbine blade are solved numerically. Using spectral/hp element method can help (1) to use the knowledge of details of flow for aero-elasticity predictions using a DNS model (2) to

significantly reduce the computation time compared to other DNS methods based on finite volume techniques, and (3) to achieve more accurate prediction of the flow separation point on the suction surface of the turbines by considering oscillations in real physical conditions.

2. Physical description

Fig. 1 shows the schematic view of the turbine blade cascade and the boundary conditions of the computational domain used in this study. It can be seen that the turbulent air flow enters horizontally $(\alpha = 0)$. Finer mesh is used in the wake region and on the suction surface of the blade to accurately capture the flow unsteadiness and flutter instabilities due to the blade's vibrations. High-order pressure outlet boundary condition is also employed at the outflow of the domain. The details of the mesh structure illustrate that 8-layers of inflated quad-mesh with the growth rate of 1.1 are implemented near the blade surface to ensure that the Δx^+ and Δy^+ values remain less than 1 during the computations. No-slip boundary conditions were implemented on the walls. The details of the geometrical and physical parameters of the blade cascade are provided in Table 1. The Reynolds number remains constant at $\mathrm{Re} = 2\times10^5$ during the computations. The chord length (C), vibration amplitude (A), vibration frequency (f) and the blade length in the span direction (L) are selected as 143mm, 0.03C, 5.2-10.3Hz, and 180mm, respectively. The geometrical parameters are selected according to the experimental study of Huang et al. [35] for validation purposes. The vibration amplitude of the blade is assumed to be linear in the span direction as suggested in the experiments. The blade vibrates in the vertical direction with the prescribed vibration amplitude.

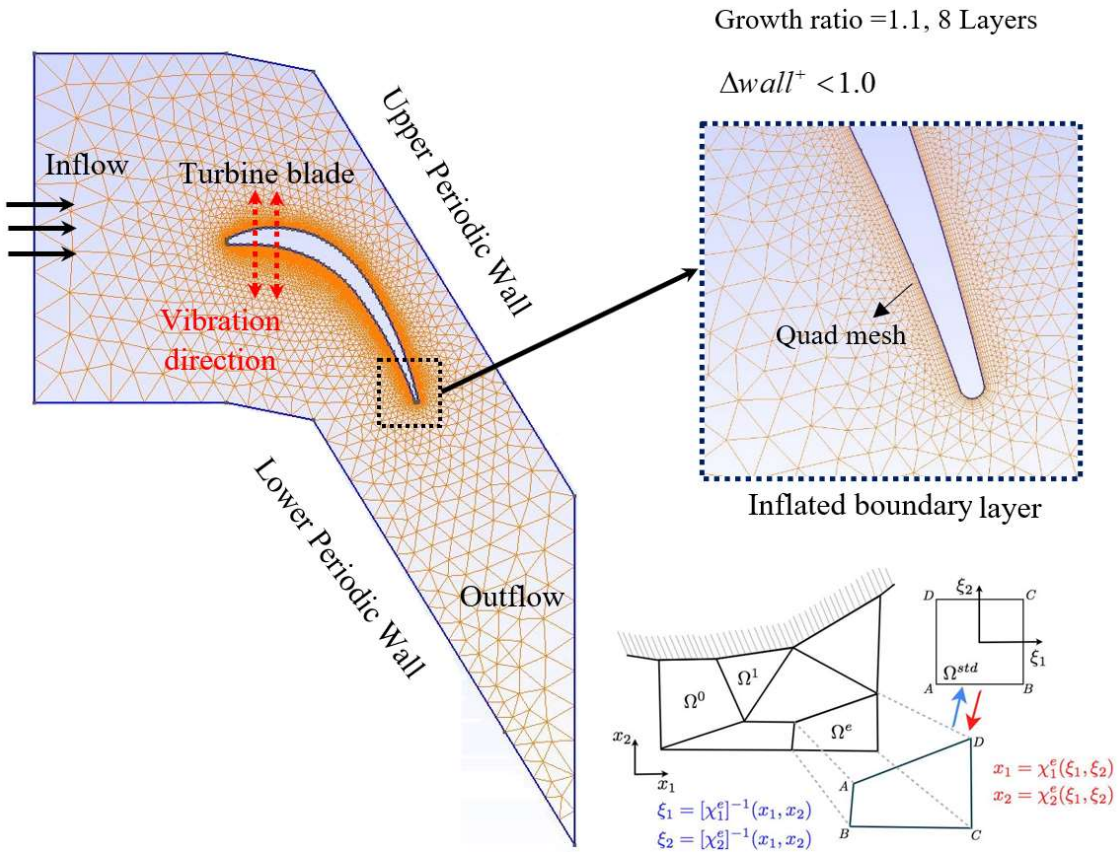

Fig. 1 Schematic of the turbine blade cascade and meshing structure

Table 1 Geometrical and Physical parameters of the blade cascade in the computational domain

Parameter	**Symbol**	**Value**
Chord	C	143mm
Inlet flow angle	α	0 degree
Vibration amplitude	A	3% chord length at blade tip
Vibration frequency	f	5.2Hz-10.3Hz
Reynolds number	Re	200,000
Blade span	L	180mm

The details of the generated mesh for polynomial order (P) of 6 over the blade cascade are shown in Fig. 2. It can be seen that by using P=6, every element will be divided into six sections on the edges of the element. Moreover, a refined mesh is used in the separation region to detect the recirculations and vortex flows in this area. Fast-Fourier-Transform (FFT) is used in span direction to extend the simulations into the Z direction. The details of the FFT transposition

and mesh decomposition in spectral/hp element method is thoroughly discussed by Serson [36]. By performing grid independency study, it was concluded that 48 Fourier surfaces in spanwise direction $\left(N_z = 48\right)$ was accurate to calculate the flow structures and pressure fluctuations for $L_z = 0.2$. In addition, higher-order pressure-outlet boundary conditions were utilized at the outflow to improve the accuracy of the computations.

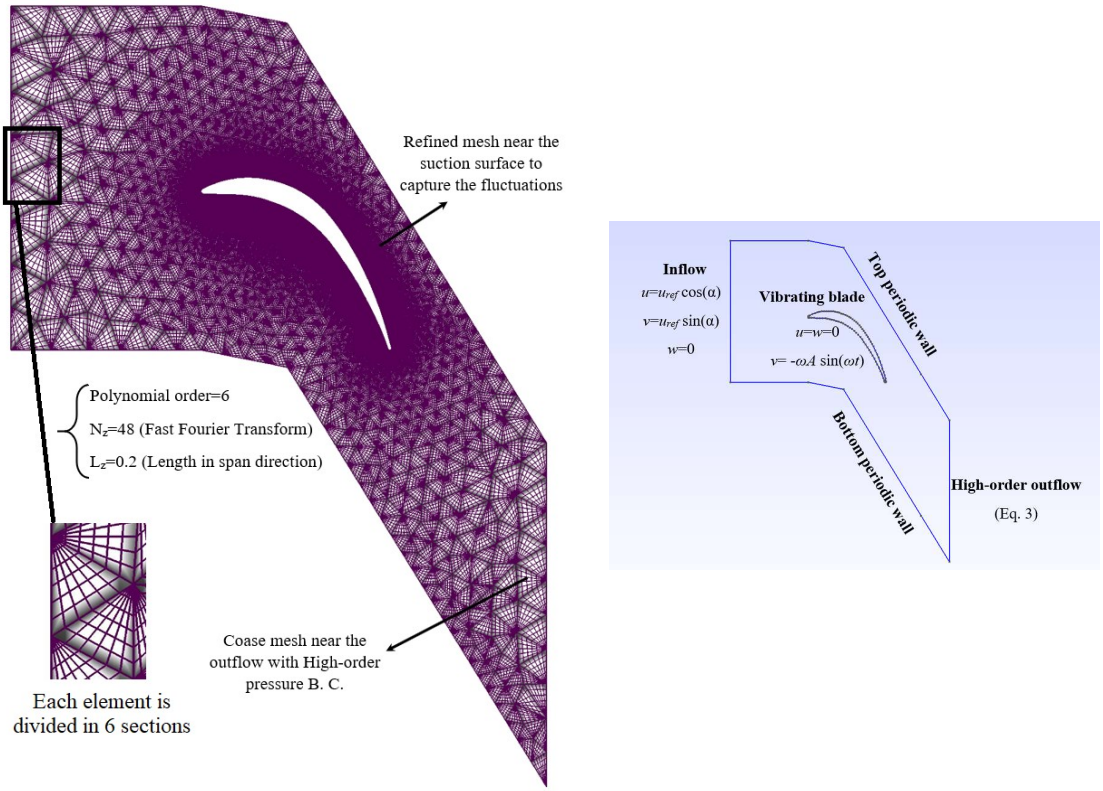

(a) (b)

Fig. 2 (a) Grid production on the blade in spectral/hp element technique, (b) boundary conditions of the model.

3. Numerical modelling

3.1. Governing equations

The 3D unsteady, and incompressible Navier-Stokes equations in the tensor form used in this analysis can be expressed by:

$$\frac{\partial \mathbf{u}}{\partial t} + (\mathbf{u}.\nabla)\mathbf{u} = -\nabla p + \nu \nabla^2 \mathbf{u} \quad (1)$$

$$\nabla.\mathbf{u} = 0 \quad (2)$$

which vector $\mathbf{u}=(u,v,w)$ illustreates the turbulent velocity of the air, p is pressure, and ν is the kinematic viscosity of air. The Re number $\left(Re = \frac{U_{in}C}{\nu}\right)$ is assumed to remain at 200,000 during the DNS analysis.

3.2. Boundary conditions

The details of the boundary conditions were presented in Fig. 2b. Periodic boundary conditions are implemented on the upper and lower walls of the domain. The inlet velocity components are also presented. When energetic vortex flows pass through the outflow region of the domain, it is essential to employ a robust and highly accurate boundary condition at the outlet. In the study of Dong et al. [37], a pressure Dirichlet outflow condition can be used as:

$$p^{n+1} = \nu \mathbf{n}.\nabla \mathbf{u}^{*,n+1}.\mathbf{n} - \frac{1}{2}\left|\mathbf{u}^{*,n+1}\right|^2 S_o\left(\mathbf{n}.\mathbf{u}^{*,n+1}\right) + \mathbf{f}_b^{\,n+1}.\mathbf{n} \quad (3)$$

The above high-order pressure outlet boundary condition is employed at the outflow of the domain. Moreover, it is presumed that the blade oscillates in y-direction only with a harmonic function.

3.3. Spectral-hp element methodology

The Spectral-hp element technique is able use a coarse and two-dimensional mesh and high accurate results can be achieved by raising the polynomial order. The simulations can be expanded in the third direction (span direction) by using the Fast Fourier Transform (See Fig. 2). Both continuous Galerkin (CG) and discontinuous Galerkin (DG) methods can be used in the solver [38] and the details of each method can be specified in the properties section of the solver code. In the present work, Galerkin method is utilized for the DNS on the oscillating turbine cascade. This technique is able to accurately discover the flow separation points and

vortex generation over different shapes even at high Reynolds numbers, where the details of the flow structure cannot be detected by employing other numerical methods. Moxey et al. [39] concluded that the spectral/hp element technique can correctly calculate the flow unsteadiness and recirculations on vibrating bodies by employing the mapping function. The details of the solution algorithm and also the relation between global domain decomposition and model-nodal expansions in the elements are provided in Fig. 3. The simulations were performed by NEKTAR++ open-source code. Calculating the highlighted terms in the solution algorithm, including Advection, Poisson and Helmholtz, requires the highest computation time compared to the other terms in the iterative unsteady analysis. The mapping function was utilized to deform the global grid into rectangular elements in the local coordinate, as already shown in Fig.1. The details of the mesh deformation can be found in [40].

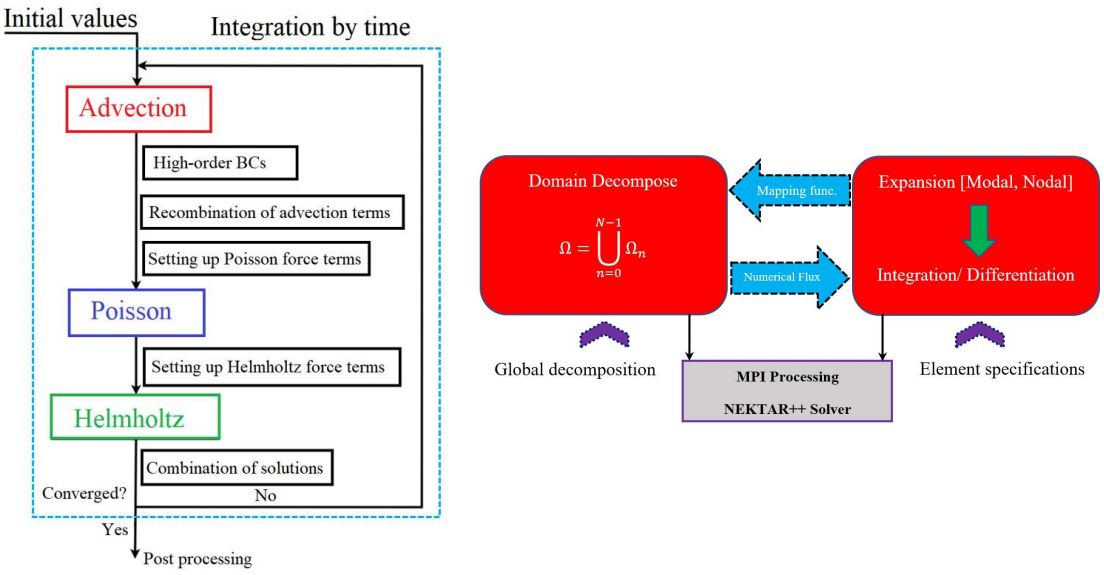

Fig. 3 Incompressible Navier-Stokes solution algorithm in spectral/hp element method, details of the domain decomposition in NEKTAR++ solver.

The momentum equation can be expressed as:

$$\frac{\partial \mathbf{u}}{\partial t} = \mathbf{N}(\mathbf{u}) + \nu \mathbf{L}(\mathbf{u}) - \nabla p \tag{4}$$

where $\mathbf{N}(\mathbf{u}) = -(\mathbf{u}.\nabla)\mathbf{u}$ and $\mathbf{L}(\mathbf{u}) = \nu\nabla^2\mathbf{u}$ are the convective viscous terms, respectively. With employing the time-integration scheme of Karniadakis et al. [41], the momentum equations can be discretised by using the backward difference formula. By discretising the convective term explicitly using polynomial extrapolations from previous time-steps, the momentum equation in time-step n+1 can be expressed as:

$$\frac{\gamma_0\mathbf{u}^{n+1} - \sum_{q=0}^{J_i-1}\alpha_q\mathbf{u}^{n-q}}{\Delta t} = \sum_{q=0}^{J_e-1}\beta_q\mathbf{N}\left(\mathbf{u}^{n-q}\right) - \nabla p^{n+1} + \nu\mathbf{L}\left(\mathbf{u}^{n+1}\right) \tag{5}$$

where J_e and J_i are the order of integration of the explicit and implicit terms. α, β and γ are the coefficients. Eq. (5) can be simplified as:

$$\frac{\gamma_0\mathbf{u}^{n+1} - u^+}{\Delta t} = N^+ - \nabla p^{n+1} + \nu\mathbf{L}\left(\mathbf{u}^{n+1}\right) \tag{6}$$

In which $u^+ = \sum_{q=0}^{J_i-1}\alpha_q\mathbf{u}^{n-q}$ and $N^+ = \sum_{q=0}^{J_e-1}\beta_q\mathbf{N}\left(\mathbf{u}^{n-q}\right)$. Following the methodology of Guermond and Shen [42] and by integrating over the domain Ω:

$$\int_\Omega \nabla p^{n+1}.\nabla\phi d\Omega = \int_\Omega\left(\frac{\mathbf{u}^+ - \gamma_0\overline{\mathbf{u}}^{n+1}}{\Delta t} + \mathbf{N}^+ - \nu\left(\nabla\times\nabla\times\mathbf{u}\right)^*\right).\nabla\phi d\Omega \tag{7}$$

where $\nabla\phi$ is a test function on the computational domain Ω. This equation illustrates the weak form of the Poisson equation, with the first term on the right side of the Eq. (7) shows a force term and the second term is higher-order Neumann boundary condition. To solve the discretised governing equations of the fluid flow over the blade cascade by using the spectral/hp element method, **u** can be expressed by [38]:

$$u^\delta(\xi,t) = \sum_n \hat{u}_n\phi_n(\xi,t) \tag{8}$$

The aim is to determine $\hat{u}_n$.The specifics of the solution algorithm based on the Galerkin method in spectral/hp element technique were provided in the flowchart of Fig. 3. Full description of the solution methodology and discretisation of each term can be found in [38].

3.4.Grid independence study

To guarantee the precision of the computations, a grid study is done prior to further simulations. Three physical parameters, including steady pressure coefficient (C_p), separation point (S_{sep}/S_0) on the suction surface and time-averaged momentum thickness (θ) were calculated on the blade cascade at Re=200,000 for different polynomial orders (Table 2). The simulations were begun with coarse polynomial order (P=4) and then continued to P=12 (finest mesh). The root-mean-square (RMS) deviations were evaluated compared to the P=12. It can be seen the relative error was substantially reduced by rising *P* from 4 to 12. It is found that polynomial order of 10 can precisely measure the main physical parameters on the model. Therefore, P=10 was selected for further DNS over the vibrating blade cascade.

Table 2 Grid independence study for C_p, S_{sep}/S_0, and θ over turbine blade for various polynomial orders compared to P = 12.

Parameter	P=4	P=6	P=8	P=10
C_p	3.28	2.17	1.05	0.29
S_{sep}/S_0	4.08	2.74	1.69	0.36
θ	12.62	6.33	2.20	0.48

Moreover, the time-step at every polynomial order must be small enough to make sure that the Courant–Friedrichs–Lewy (CFL) number remain less than one in each time step. The CFL parameter can be expressed by:

$$CFL = U\Delta t / h \tag{9}$$

where U, Δt and h are the air velocity, time step size, and mesh size. The maximum value of this parameter will be reported at each time step, and the computations would be stopped in this parameter exceeds 1. Based on the definition of the CFL parameter, it has a linear

dependency to the Reynolds number and therefore, the time-step must be small enough at high Reynolds numbers until the simulations remain convergent during the computations. The simulations revealed that the time-step size of 2.5×10^{-5} would be small enough to remain convergent for the highest polynomial order used in the present DNS analysis (P=12).

4. Results and discussion

4.1. Validation with experiments

Validations is essential in creating certainty in the numerical analysis and hence the discussions provided for the numerical results. The transient flow in turbine cascade because of controlled vibrations was measured experimentally by Huang et al. [35] to advance knowledge of turbine blades aeroelasticity and present accurate experimental results for validation of the numerical model in aeroelasticity simulation. This experimental data is used for validation of the numerical method in this study. So, before performing further simulations, the accuracy of the DNS model is validated using experimental data. The transient flow fields in the turbine linear cascade due to the blades oscillations were experimentally measured by Huang et al. [35]. The Reynolds number is kept constant at Re=200,000 and the oscillation amplitude is 3% of the chord length at the blade tip and 0.3% chord at hub. The experimental results are used for the purpose of validation of the numerical method in this study. Fig. 4 shows the comparisons of the numerical results with experimental data [35] for time-averaged pressure coefficient over the blade cascade at 50% span.

Based on the grid independency study in the previous section, the polynomial order in spectral/hp element method is selected as P=10. The time-averaged pressure coefficient, C_p, is defined as $(P_s - P_o)/(P_{total\text{-}i}-P_o)$, in which P_s is the time averaged values of blade static pressure, P_o is the reference pressure at the outlet, and $P_{total\text{-}i}$ is the total pressure at the inlet of the test section. It can be seen that the numerical results are in excellent agreement with experimental data on both of the suction surface (S.S.) and pressure surface (P.S.) of the blade cascade. The

results are plotted as functions of the axial chord length of the blade. The fluctuations in the pressure coefficient detected near the trailing edge are due to the unfavourable pressure gradient and flow separation in this region.

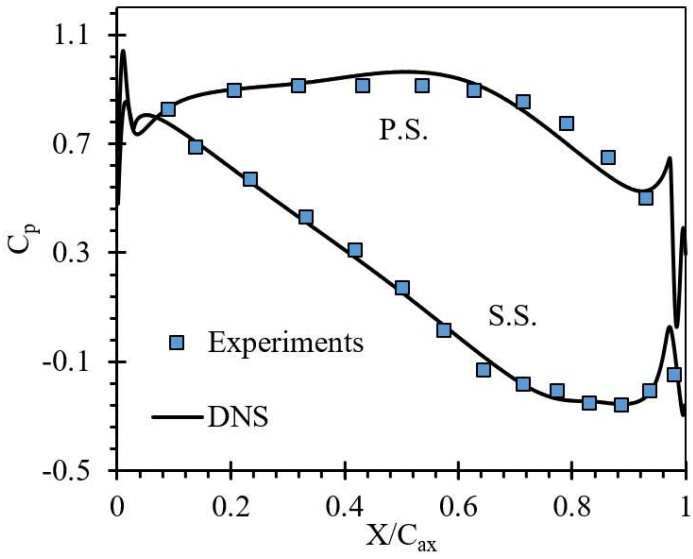

Fig. 4 Validation of the time-averaged pressure coefficient over the blade with experiments [35] for Re=200,000.

The flow solution variables such as velocity and pressure are obtained as time series using the DNS method. To analyse the disturbances due to the blade vibration, the aerodynamic solution parameters over the blade cascade, Q can be expressed by [43]:

$$Q = \bar{Q} + A_Q \cos(\omega t) + B_Q \sin(\omega t) \tag{10}$$

where $\bar{Q}$, A_Q and B_Q are the Fourier coefficients of the conservation parameters and $\omega = 2\pi f$ is the vibration frequency. $\bar{Q}$ is the time-averaged value over a period of vibration frequency. A temporal Fourier transform is used to calculate the Fourier components (A_Q and B_Q) as follows [43]:

$$A_Q = \frac{\omega}{\pi} \sum_{i=1}^{n} (Q_i) \mathrm{Sin}(\omega t_i) \Delta t_i \tag{11-a}$$

$$B_Q = \frac{\omega}{\pi}\sum_{i=1}^{n}\left(Q_i\right)\mathrm{Cos}\left(\omega t_i\right)\Delta t_i \tag{11-b}$$

$$\bar{Q} = \frac{\omega}{2\pi}\sum_{i=1}^{n}\left(Q_i\right)\Delta t_i \tag{11-c}$$

In the above equations n is the number of time instances of the series and $\bar{Q}$ shows the time averaged values. It should be pointed out that only the first harmonic of the flow parameters is considered in the present simulations.

When the turbine blade oscillates with a specific frequency, the time dependent pressure can be expressed as $P = \bar{P} + P_A\cos\left(\omega t\right) + P_B\sin\left(\omega t\right)$, where $\bar{P}$ is the average steady pressure and P_A and P_B are unsteady coefficients. Consequently, the unsteady pressure amplitude $\tilde{p}$ and phase angle $\left(\phi\right)$ can be expressed as $\sqrt{P_A^2 + P_B^2}$ and $\tan^{-1}\left(P_B / P_A\right)$, respectively.

To show the accuracy of the obtained direct numerical results for the unsteady pressure coefficient over the blade cascade, a comparison with experiments is provided in Fig. 7. The results are compared with the experiments [35] for the vibration frequency of 5.2Hz (reduced frequency=0.2) for inner blade phase angle (IBPA) equal to 0. It can be seen that the results are in good agreement with the experiments, especially on the pressure surface of the blade at different span.

Fig. 5 illustrates the effects of vibration frequency on the unsteady pressure amplitude over both suction surface and pressure surface of the blade cascade. It can be seen that the unsteady pressure amplitude over the suction surface is higher than the pressure surface. The results illustrate that C_{p1} augments in the span direction. This is mainly due to the linear vibrations of the blade which has the highest amplitude at the blade tip (3% chord length). The additional fluctuations and recirculation flows intensifies the unsteady pressure coefficient on both the upper and lower side of the blade cascade. Some deviations are observed between the experimental data and DNS results on the suction surface of the blade, which may be due to the strong vortex production and recirculating flows in separated region on the oscillating blade

surface. These deviations are considerable near the flow separation point. However, most of the deviations between the experimental data and the numerical results become negligible at $X/C_{ax}>0.6$.

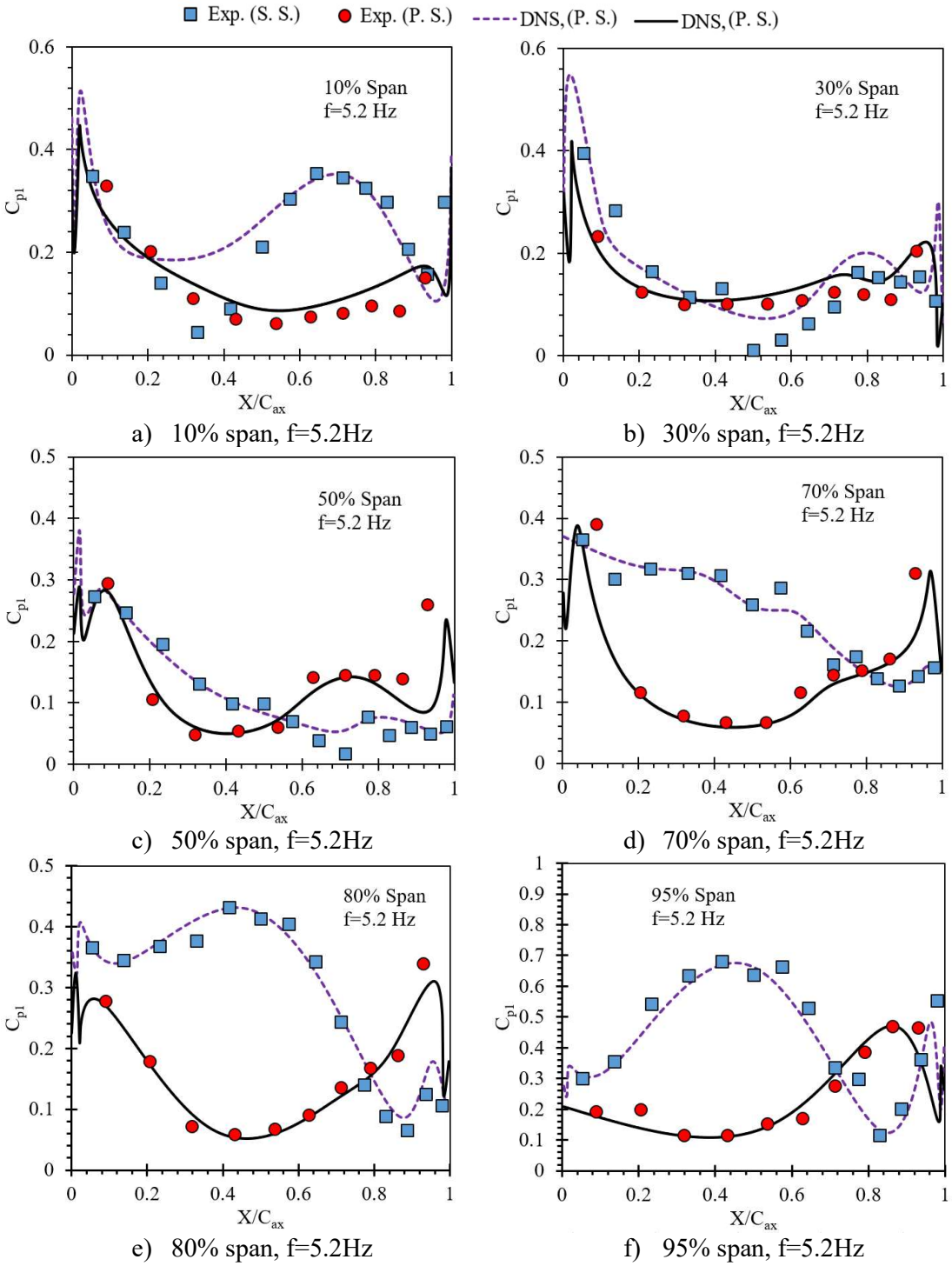

a) 10% span, f=5.2Hz b) 30% span, f=5.2Hz

c) 50% span, f=5.2Hz d) 70% span, f=5.2Hz

e) 80% span, f=5.2Hz f) 95% span, f=5.2Hz

Fig. 5 Validation of the numerical data with experiments [44] for C_{p1} at different spans.

Fig. 6 shows a comparison between the DNS results of the present study and experimental data [35, 44] for the pressure phase angle variations for the vibration frequency of f=5.2Hz. As can be seen, the variations of the phase angle in the span direction is small and negligible. Similar trend for the phase angle variations over the oscillating blade was observed in the experiments. The variations of the phase angle near the trailing edge of the blade are due to the flow separation and recirculating flows in this region. The unsteady pressure phase angle varies between ±80 degrees on the suction surface for different span sections. It can be seen that the phase angle increases by moving forward in the span direction. This is mainly due to the strong recirculation flows generated over the suction surface of the blade with higher vibration amplitudes near the blade tip. More physical details about the flow structure over the vibrating blades with different vibration amplitudes were provided in the previous sections.

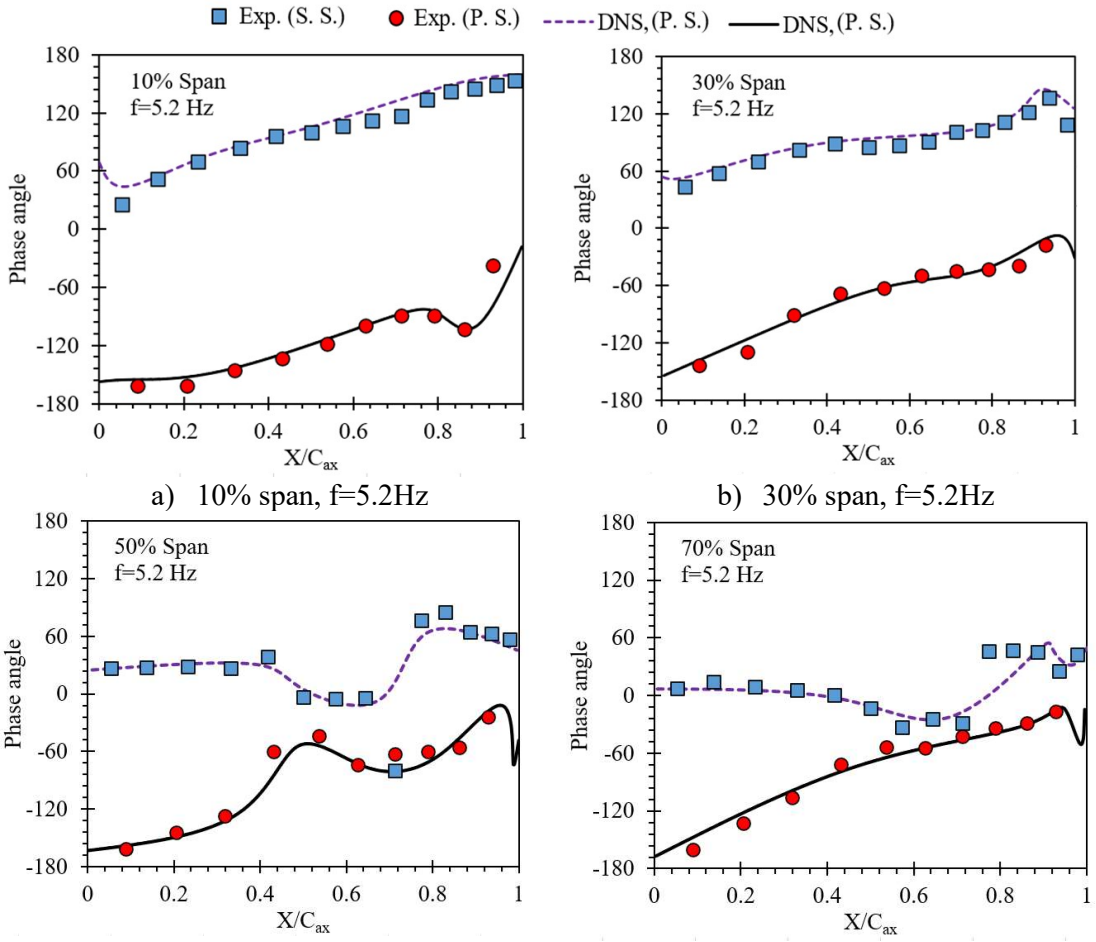

a) 10% span, f=5.2Hz b) 30% span, f=5.2Hz

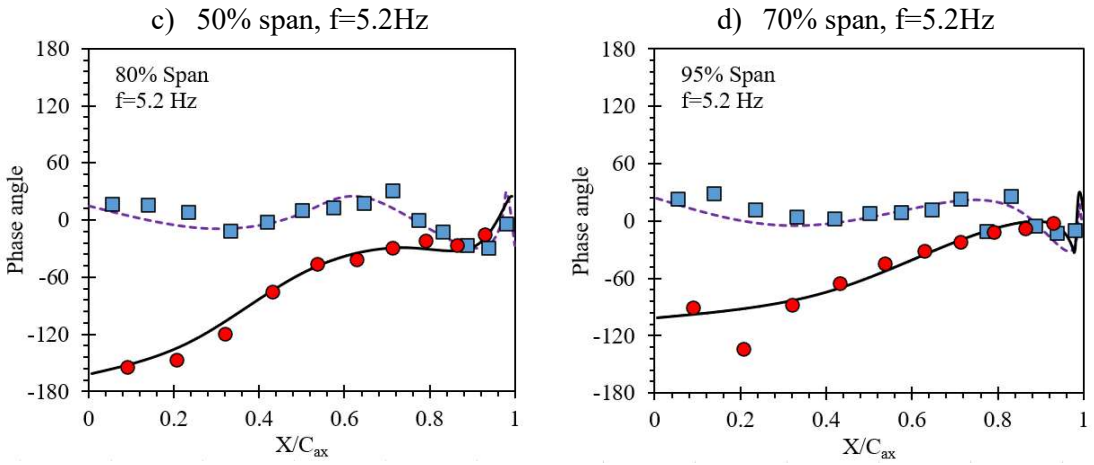

Fig. 6 Validation of the numerical data with experiments [44] for phase angle at different span sections.

4.2.Effects of vibrations on turbulent flow structure

Fig. 7 depicts the iso-surface contours of dimensionless span vorticity $\left(w_z = 50\right)$ as functions of axial velocity over stationary and oscillating blade cascade at Re=200,000. The iso-surfaces are plotted as functions of the dimensionless axial air velocity (u). The DNS results show that stronger vorticity can be detected over the vibrating blade in comparison with the stationary blade without oscillations. The main reason for stronger vortex generations and recirculation over the vibrating blade is due to the flow separation and shear-layer on the turbine blade cascade. More details about the vortex shedding affected by the flow separation near the trailing edge of the blade are also detected in the DNS simulations. It can be seen that size of the eddies passing over the blades suction surface become larger in the presence of vibrations with f=5.2Hz. The size and shape of the vortex shedding close to the trailing edge separating point is different between the stationary and vibrating blade because of the stronger air velocity magnitude detected over the oscillating blade. Laminar vortex shedding from the trailing edge, of which the flow structure is similar to that of Karman vortex, is dominant within the initial periods. The separation of shear layers and the evolution of coherent structures are observed as

time goes on. The rolling up and break down of the separated shear layers because of Kelvin-Helmholtz instabilities leads to a transition to the turbulent flow near the trailing edge.

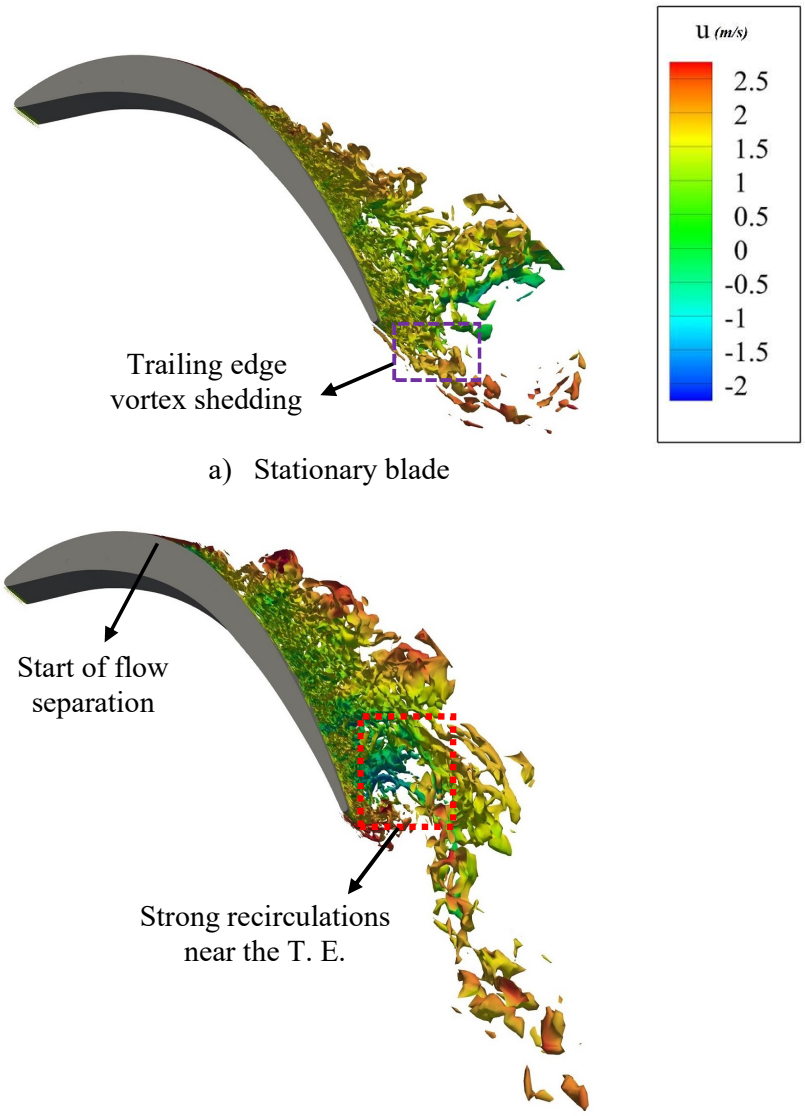

a) Stationary blade

b) Vibrating blade, f=5.2 Hz

Fig. 7 Iso-contours of vorticity on stationary and oscillating turbine blade.

Fig. 8 shows the impact of the oscillation frequency on spanwise vorticity contours (w_z) over the turbine blade cascade at 30% span. It can be seen that the boundary layer disruptions grow significantly by raising the vibration frequency from 0 to 10.3Hz. Furthermore, it was observed that the vortex shedding around the trailing edge of the blade becomes stronger over the suction surface of the oscillating blades. As can be seen, strong instantaneous recirculation flow is

generated in the wake area of the oscillating blade with higher frequencies which is mainly due to the flow disturbance and fluctuations generated over the vibrating surface with f=10.3Hz.

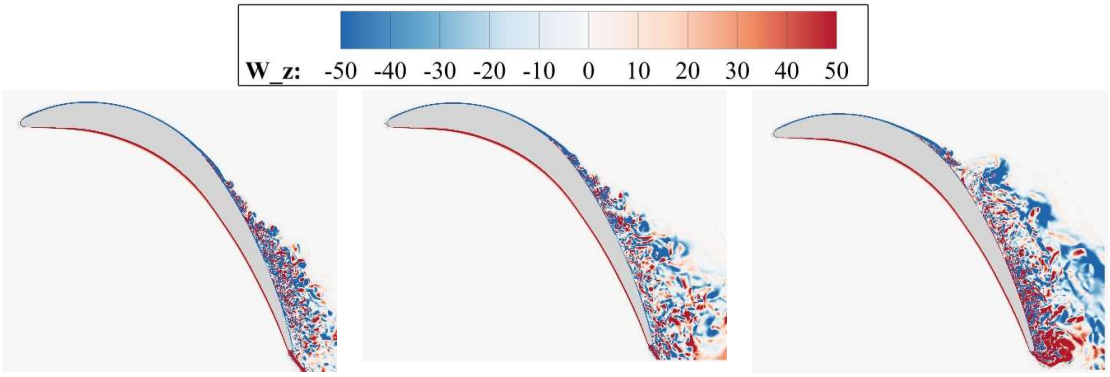

a) Stationary blade

b) Oscillating blade (f=5.2 Hz)

c) Oscillating blade (f=10.3 Hz)

Fig. 8 Effects of the vibration frequency on vorticity generations over blade cascade at Re=200,000 at 30% span.

The unsteady pressure coefficient and phase angle for the vibration frequency of 10.3Hz at different span sections are provided in Fig. 9. It can be seen that the unsteady pressure coefficient is very high near the leading edge ($X/C_{ax} \approx 0$) of the blade. The results show that the unsteady pressure coefficient raises on the suction surface of the blade, and after the flow separation occurrence ($X/C_{ax}>0.40$) it decreases. By comparing the C_{p1} data at four different span sections, it can be deduced that the unsteady pressure coefficient is highest at 70% span. Physically speaking, this is mainly due to the higher vibration amplitude at higher span sections which results in stronger recirculation flows and vortex generations on the suction surface of the blade. Stronger recirculation flows intensify the pressure coefficient. Moreover, some fluctuations are detected near the trailing edge of the blade which is a result of the adverse pressure gradient at high Reynolds numbers. The variation of the pressure coefficient on the pressure surface of the oscillating blade is more uniform. This is because the flow separation occurs on the suction surface, which significantly impacts the pressure coefficient in this region.

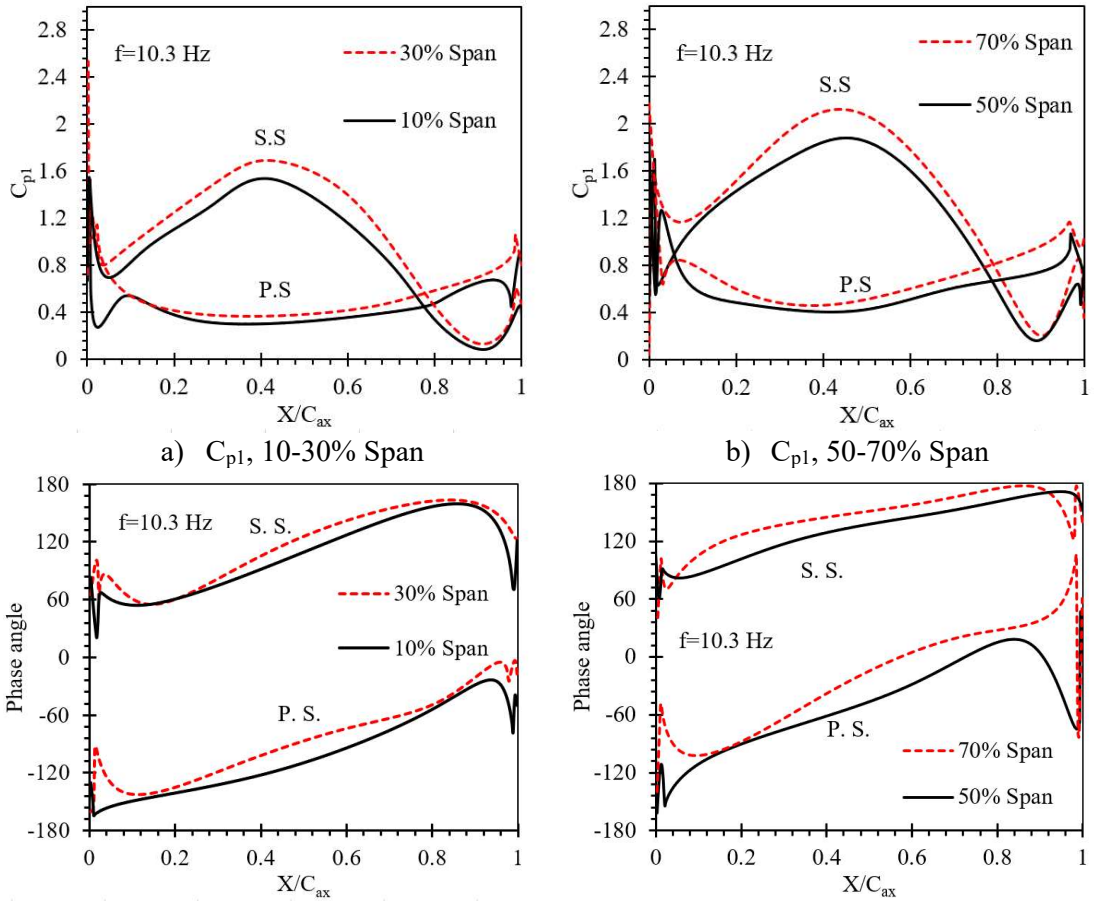

a) C_{p1}, 10-30% Span b) C_{p1}, 50-70% Span

c) Phase angle, 10-30% Span d) Phase angle, 50-70% Span

Fig. 9 Unsteady pressure amplitude coefficients at vibration frequency of 10.3Hz at different spanwise sections.

The effects of vibrations on the wall shear stress (WSS) over the turbine blade surface at 50% span are provided in Fig. 10. Strong wall shear stress is detected behind the leading edge of the blade in both stationary and oscillating cases. This intensified WSS near the leading edge is due to the starting of interaction between the blade structure and the turbulent flow. It can be seen that after occurring the flow separation over the suction surface of the blade cascade, additional wall shear stress is observed, which is due to the adverse pressure gradient. The additional vortex production and recirculating flows on the oscillating blade intensify the shear stress over the blade surface. Moreover, the wave packets generated in the turbulent boundary layer over the oscillating blade enhance the wall shear stress in this area.

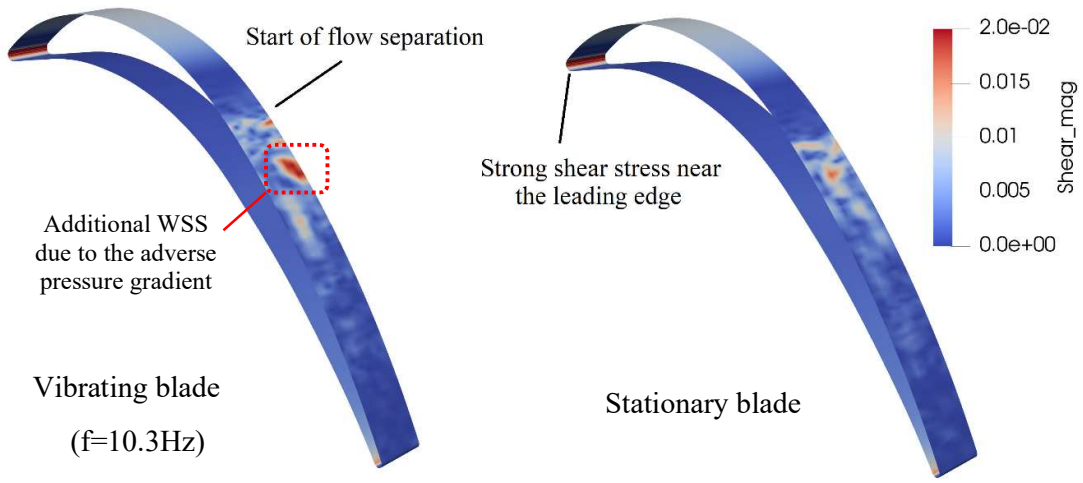

Fig. 10 The effects of blade vibrations on wall shear stress contours at the 50% span over turbine blade at Re=200,000.

Fig. 11 depicts the transient momentum thickness profiles (θ) over the suction surface of vibrating blades at different spans and also stationary blade. The momentum thickness can be expressed as:

$$\theta = \int_{y=0}^{\delta} \frac{u}{U_\infty}\left(1-\frac{u}{U_\infty}\right)dy \tag{12}$$

where U_∞ is the constant velocity of the turbulent flow in the far field. The results are provided for three harmonic vibration periods $(0 < t^* < 3)$ for vibration frequency of f=10.3Hz at the dimensionless location of s/S_0=0.90. The results illustrate that the momentum thickness grows in the spanwise direction. The highest value of the momentum thickness at 90% span is 0.0091 which is 40% higher compared to the highest value of this parameter at 10% span $(\theta = 0.0065)$. It can be seen that the average momentum thickness over all of the oscillating blades is higher than the stationary blade. This is mainly due to the additional recirculating flows and instabilities over the oscillating blade. The average values of the momentum thickness at 10, 50, and 90% span of the oscillating blade are 11.2%, 53.3%, and 61.2%, respectively higher

than the stationary blade cascade. The momentum thickness is increased because of the bigger separation bubbles which have considerable impact on the wave packets. The hydraulic boundary layer thickness growth near the trailing edge of the oscillating blades compared to the stationary one, is due to the faster flow separation of turbulent flow over the vibrating blade cascade. When the flow separation occurs faster on the suction surface of the blade, the turbulent wetted region will be intensified and therefore, the momentum loss raises in the boundary layer region. The calmed regions indicate the flow detachment and reattachment on the suction side of the vibrating blade in a vibration period which has similar behaviour to the harmonic vibration functions of the blade surface.

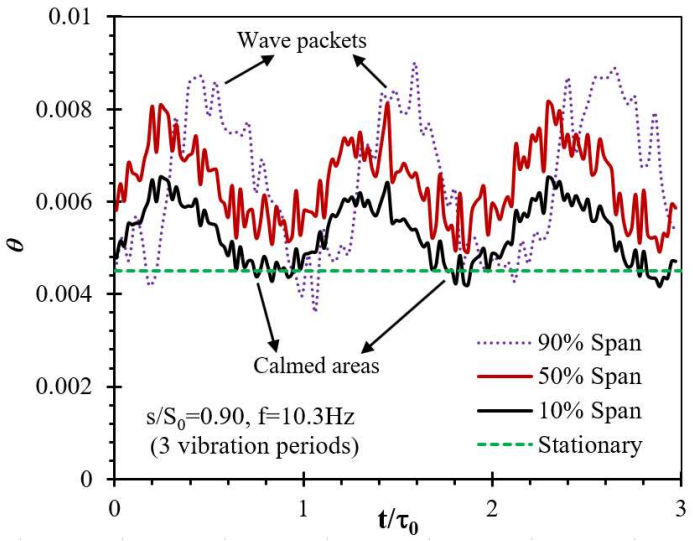

Fig. 11 Momentum thickness profiles over oscillating blade cascade at different spanwise directions at Re=200,000.

The effects of vibration frequency on instantaneous dimensionless pressure contours and surface streamlines at 50% span of the blade cascade at $\mathrm{Re}=2\times10^5$ is shown in Fig. 12. It can be seen that some counter-clockwise recirculations are generated near the trailing edge of the oscillating turbine blade at a higher vibration frequency (f=10.3Hz). These recirculations are mainly due to the additional boundary-layer disruptions and pressure fluctuations on the

suction surface of the vibrating blade. The dimensionless pressure P^* is defined as $P^* = P/\left(1/2\rho_{ref}u_{ref}{}^2\right)$ in which ρ_{ref} and u_{ref} are the reference density and fluid velocity, respectively. The reference values are evaluated at 0.3C upstream of the blade cascade inlet. The regions with blue contours show the adverse pressure gradient effects on the vortex generations and turbulent flow recirculations. Moreover, it can be seen that the vortex shedding caused by flow separation on the suction surface is clockwise, while the direction of the vortex shedding near the trailing edge of the blade with higher vibration frequency (Case b) is anti-clockwise. A low-pressure region covers the suction surface of the blades, which is wider at f=10.3 Hz than in f=5.2 Hz. Accurate detection of this area is essential because the transition of the separated turbulent flow has occurred near the point of lowest pressure on the suction side. It can be seen in Fig. 11-b the instantaneous separation bubbles shift the recirculation flow direction and deviate the vortex shedding flow angle from its structure over the stationary blade.

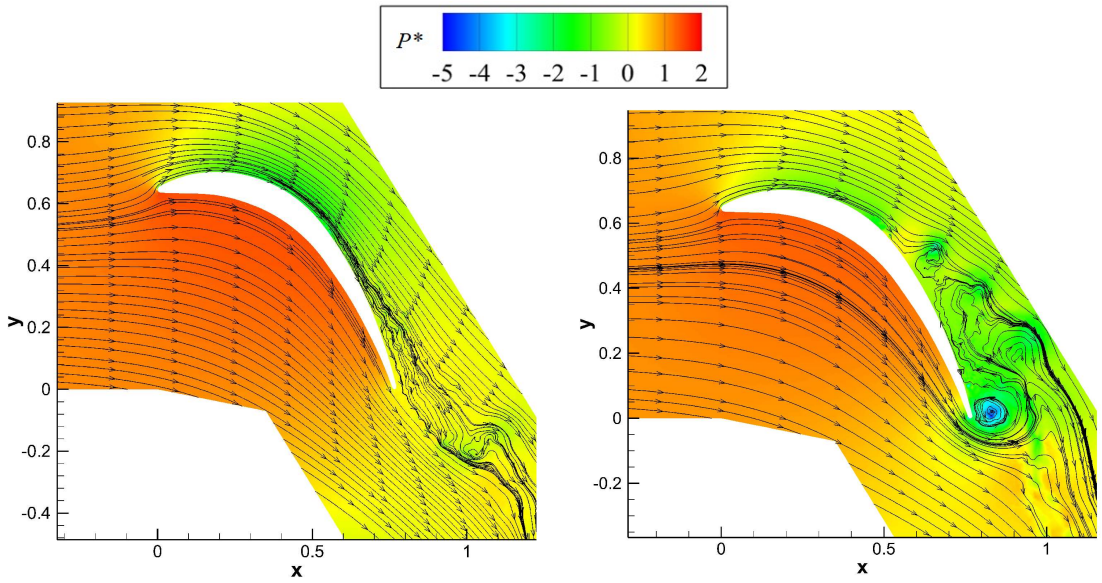

a) f=5.2 Hz b) f=10.3 Hz

Fig. 12 Dimensionless instantaneous unsteady pressure contours at the 50% span over turbine blade at Re=200,000.

To better describe the main physical reasons for flow separation and vortex generation over the stationary and oscillating turbine blade cascade, the instantaneous vorticity contour is presented in Fig. 13. The results are provided for $\mathrm{Re}=2\times10^5$ after 10,000 vibration periods. It can be seen that the separation point over the stationary blade is at S_{sep}/S_0=0.391 which is reduced to S_{sep}/S_0=0.372 over the vibrating blade. As discussed earlier, the vortex shedding caused by flow separation on the suction surface is clockwise, while the direction of the vortex shedding near the trailing edge of the blade with higher vibration frequency is anti-clockwise, and it is much higher than the other transitional recirculations on the suction surface of the oscillating blades. Turbulent boundary layer destruction and stronger adverse pressure gradient over the suction side of the vibrating blade with f=10.3 Hz are the main reasons for 5.1% reduction in flow separation point compared to the oscillating blade with f=5.2 Hz.

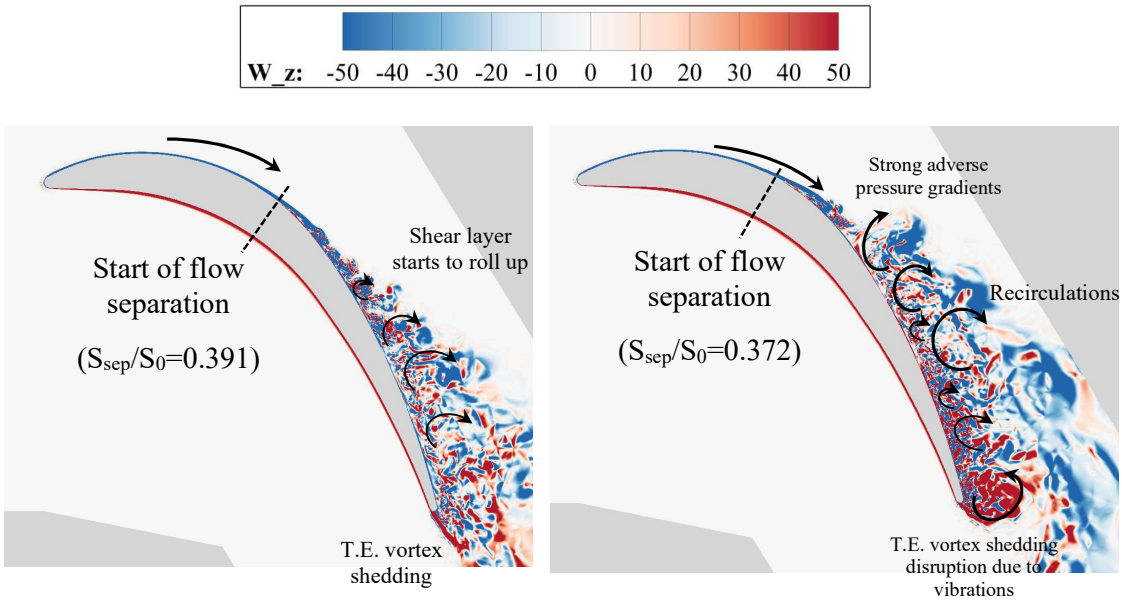

a) f= 5.2 Hz b) f= 10.3 Hz

Fig. 13 Details of the flow structures and separation point on stationary and vibrating turbine blade cascade

4.3. PSD profile and Parallel processing

The impact of blade oscillations on the power spectral density (PSD) profile of the pressure signals in the wake region is shown in Fig. 14. The averaging periodogram methodology [45] is utilised in the computations to calculate the PSD magnitude. More information about the methodology of calculating this parameter is available in Ref. [46]. The PSD of any variable K is expressed as [46]:

$$PSD(St) = \frac{2\left(\hat{K}\right)^2}{\Delta\left(f\ C/U_{in}\right)} = \frac{2\left(\hat{K}\right)^2}{\Delta(St)} \tag{12}$$

where St, f and C are Strouhal number, frequency, and the chord length, respectively. $\hat{K}$ denotes the scale of the parameter that is computed by carrying out Fourier transform of the signals. The results show that the PSD of the pressure signal for all of the stationary and vibrating blade with different vibration frequencies at Re=200,000 fall below the -5/3 line. The results show that the convergency of the simulations for all of the cases is achieved at Strouhal numbers higher than 80. This is one of the main advantages of the spectral/hp element method to perform DNS over vibrating blades without instability issues observed in the finite volume method (FVM) and other numerical methods.

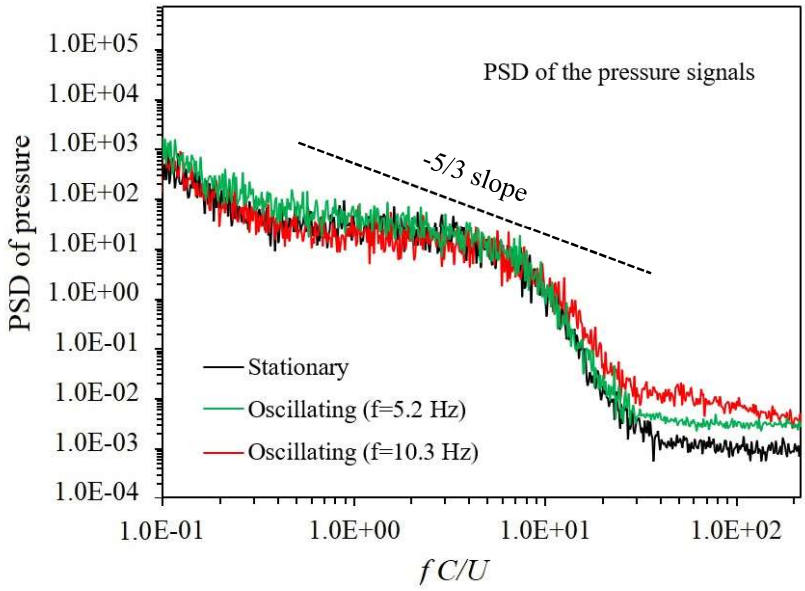

Fig. 14 Comparison between PSD of the pressure signals in the wake region of the stationary and oscillating blades with P = 10 at Re = 200,000

Fig. 15 shows the contours of the computations speedup by using parallel processing compared to the single process. To perform DNS over blade cascade, different number of processors can be used in X-Y planes and also in span direction (Z). As can be seen, the computation time can be reduced up to 600-timers compared to the single processing on the local HPC cluster. Moreover, increasing P_{XY} from 1 to 16 does not have considerable impact on the computation time reductions, but huge computation time reduction could be achieved by raising the P_{XY} from 64 to 128. It should be pointed out the computation efficiency is another parameter that should be considered in the computations. Using a higher number of processors will result in longer queues on the cluster and higher resources expenditure. It was observed that using 64 processors in XY, and eight processors in Z direction, will provide enough speed and acceptable efficiency.

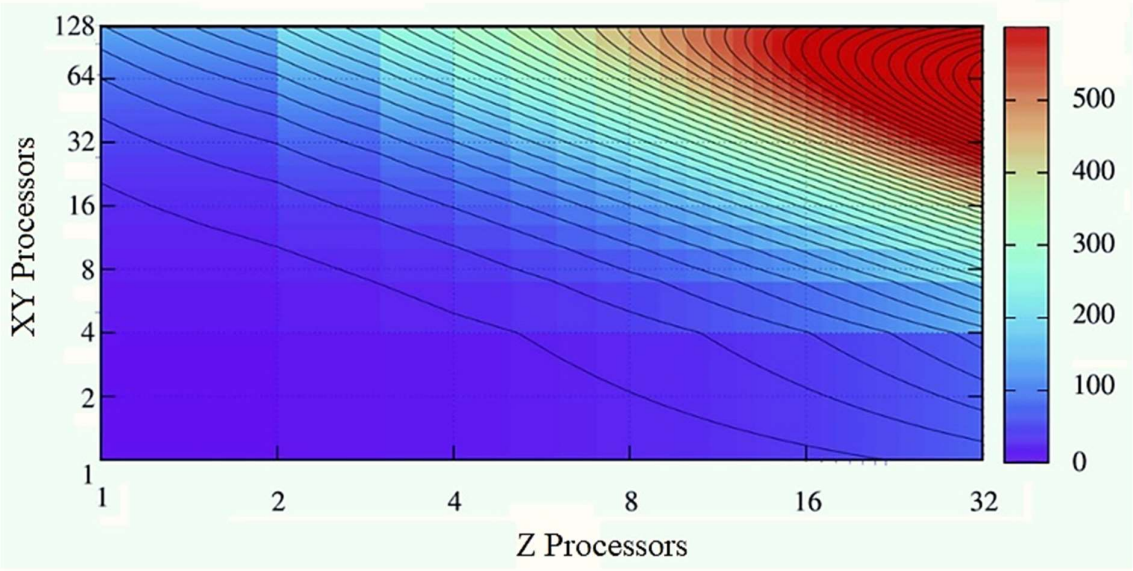

Fig. 15 Computation time speedup in parallel processing compared to the single processing over oscillating blade cascade at Re=200,000.

5. Conclusion

In the present study, direct numerical simulations have been performed to investigate aerodynamic phenomena such as flow separation, vortex shedding, and momentum thickness over stationary and oscillating turbine blades. The simulations were performed at $\mathrm{Re}=2\times10^5$ and at different span sections with two different vibration frequencies $\left(f=5.2,10.3Hz\right)$. The main conclusions of this study are:

- Stronger vorticity generations were detected over the oscillating blade in comparison with the stationary turbine blade. The main physical reason for the additional vortex production and flow recirculations on the oscillating blades is faster flow separation and shear-layer on the turbine blade cascade.
- The boundary layer disruption and unsteady fluctuations grow significantly by raising the blades vibration frequency from 0 to 10.3Hz. Furthermore, it was observed that the vortex shedding around the trailing edge of the blade becomes stronger over the suction surface of the oscillating blades.
- The flow separation over the suction surface of the stationary blade occurs at S_{sep}/S_0=0.391 while it occurs at S_{sep}/S_0=0.372 over the vibrating blade with *f*=5.2 Hz. Moreover, the vortex shedding caused by flow separation on the suction side is clockwise, while the direction of the vortex shedding near the trailing edge with higher vibration frequency is anti-clockwise.
- Turbulent boundary layer destruction and stronger adverse pressure gradient over the suction side of the vibrating blade with f=10.3 Hz are the main reasons for 5.1% reduction in flow separation point compared to the oscillating blade with f=5.2 Hz.
- The results showed that C_{p1} augments in the span direction. The additional fluctuations and recirculation flow intensifies the unsteady pressure coefficient on both the upper

and lower side of the blade cascade. A similar trend was observed in pressure phase angle variations.

- The momentum thickness grows in the span direction. The maximum value of the momentum thickness at 90% span is 0.0091, which is 40% higher compared to the highest value of this parameter at 10% span $(\theta = 0.0065)$. The average values of the momentum thickness at 10, 50, and 90% span of the oscillating blade are 11.2%, 53.3%, and 61.2%, respectively, higher than the stationary blade cascade.
- A low-pressure region covers the suction surface of the blades, which is wider at f=10.3Hz than in f=5.2Hz.

References

[1] H. Li, K. Ekici, A novel approach for flutter prediction of pitch–plunge airfoils using an efficient one-shot method, Journal of Fluids and Structures, 82 (2018) 651-671.
[2] M. Giles, UNSFLO: A numerical method for the calculation of unsteady flow in turbomachinery, Cambridge, Mass.: Gas Turbine Laboratory, Massachusetts Institute of …, 1991.
[3] L. He, Harmonic solution of unsteady flow around blades with separation, AIAA journal, 46 (2008) 1299-1307.
[4] K.C. Hall, J.P. Thomas, W.S. Clark, Computation of unsteady nonlinear flows in cascades using a harmonic balance technique, AIAA journal, 40 (2002) 879-886.
[5] M. Bovand, S. Rashidi, J. Esfahani, R. Masoodi, Control of wake destructive behavior for different bluff bodies in channel flow by magnetohydrodynamics, The European Physical Journal Plus, 131 (2016) 1-13.
[6] S. Rashidi, M. Bovand, J. Esfahani, H. Öztop, R. Masoodi, Control of wake structure behind a square cylinder by magnetohydrodynamics, Journal of Fluids Engineering, 137 (2015).
[7] F.M. Besem, R.E. Kielb, Influence of the tip clearance on a compressor blade aerodynamic damping, Journal of Propulsion and Power, 33 (2017) 227-233.
[8] M. Rahmati, L. He, R. Wells, Interface treatment for harmonic solution in multi-row aeromechanic analysis, Turbo Expo: Power for Land, Sea, and Air, 2010, pp. 1253-1261.
[9] M. Rahmati, L. He, D. Wang, Y. Li, R. Wells, S. Krishnababu, Non-linear time and frequency domain methods for multi-row aeromechanical analysis, Turbo Expo: Power for Land, Sea, and Air, American Society of Mechanical Engineers, 2012, pp. 1473-1485.
[10] S. Win Naung, M. Rahmati, H. Farokhi, Aerodynamic Analysis of a Wind Turbine With Elevated Inflow Turbulence and Wake Using Harmonic Method, International Conference on Offshore Mechanics and Arctic Engineering, American Society of Mechanical Engineers, 2019, pp. V010T009A062.
[11] S. Win Naung, M. Rahmati, H. Farokhi, Aeromechanical Analysis of Wind Turbines Using Non-Linear Harmonic Method, International Conference on Offshore Mechanics and Arctic Engineering, American Society of Mechanical Engineers, 2019, pp. V010T009A060.

[12] M. Vahdati, G. Simpson, M. Imregun, Mechanisms for wide-chord fan blade flutter, Journal of Turbomachinery, 133 (2011).
[13] C.D. Peters, S.J. van der Spuy, D.N. Els, J. Kuhnert, Aerodynamic damping of an oscillating fan blade: Mesh-based and meshless fluid structure interaction analysis, Journal of Fluids and Structures, 82 (2018) 173-197.
[14] S. Rashidi, M. Hayatdavoodi, J.A. Esfahani, Vortex shedding suppression and wake control: A review, Ocean Engineering, 126 (2016) 57-80.
[15] A.J. Chorin, A numerical method for solving incompressible viscous flow problems, Journal of computational physics, 135 (1997) 118-125.
[16] A.T. Wijayanta, A localized meshless approach using radial basis functions for conjugate heat transfer problems in a heat exchanger, International Journal of Refrigeration, 110 (2020) 38-46.
[17] B. Lakshminarayana, Fluid dynamics and heat transfer of turbomachinery, John Wiley & Sons1995.
[18] C. Rhie, W.L. Chow, Numerical study of the turbulent flow past an airfoil with trailing edge separation, AIAA journal, 21 (1983) 1525-1532.
[19] Y. Wang, F. Chen, H. Liu, H. Chen, Large eddy simulation of unsteady transitional flow on the low-pressure turbine blade, Science China Technological Sciences, 57 (2014) 1761-1768.
[20] Z. Ma, P. Zeng, L. Lei, Analysis of the coupled aeroelastic wake behavior of wind turbine, Journal of Fluids and Structures, 84 (2019) 466-484.
[21] J.-B. Tô, N. Simiriotis, A. Marouf, D. Szubert, I. Asproulias, D.M. Zilli, Y. Hoarau, J.C.R. Hunt, M. Braza, Effects of vibrating and deformed trailing edge of a morphing supercritical airfoil in transonic regime by numerical simulation at high Reynolds number, Journal of Fluids and Structures, 91 (2019) 102595.
[22] D. Apsley, P. Stansby, Unsteady thrust on an oscillating wind turbine: Comparison of blade-element momentum theory with actuator-line CFD, Journal of Fluids and Structures, 98 (2020) 103141.
[23] S. Rashidi, M. Bovand, J.A. Esfahani, Application of magnetohydrodynamics for suppressing the fluctuations in the unsteady flow around two side-by-side circular obstacles, The European Physical Journal Plus, 131 (2016) 1-12.
[24] P. Tucker, Computation of unsteady turbomachinery flows: Part 1—Progress and challenges, Progress in Aerospace Sciences, 47 (2011) 522-545.
[25] P.G. Tucker, Unsteady computational fluid dynamics in aeronautics, Springer Science & Business Media2013.
[26] C. Müller, R.-D. Baier, J.R. Seume, F. Herbst, DNS-based analysis of RANS predictions of a low-pressure turbine cascade, Turbo Expo: Power for Land, Sea, and Air, American Society of Mechanical Engineers, 2016, pp. V02CT39A046.
[27] T. Zaki, J. Wissink, P. Durbin, W. Rodi, Direct computations of boundary layers distorted by migrating wakes in a linear compressor cascade, Flow, turbulence and combustion, 83 (2009) 307-322.
[28] A.P. Wheeler, R.D. Sandberg, N.D. Sandham, R. Pichler, V. Michelassi, G. Laskowski, Direct numerical simulations of a high-pressure turbine vane, Journal of Turbomachinery, 138 (2016).
[29] K. Ogino, H. Mamori, N. Fukushima, K. Fukudome, M. Yamamoto, Direct numerical simulation of Taylor–Couette turbulent flow controlled by a traveling wave-like blowing and suction, International Journal of Heat and Fluid Flow, 80 (2019) 108463.
[30] T. Watanabe, X. Zhang, K. Nagata, Direct numerical simulation of incompressible turbulent boundary layers and planar jets at high Reynolds numbers initialized with implicit large eddy simulation, Computers & Fluids, 194 (2019) 104314.

[31] G. Karniadakis, S. Sherwin, Spectral/hp element methods for computational fluid dynamics, Oxford University Press2013.
[32] S.J. Sherwin, M. Ainsworth, Unsteady Navier–Stokes solvers using hybrid spectral/hp element methods, Applied Numerical Mathematics, 33 (2000) 357-363.
[33] Y. Bao, R. Palacios, M. Graham, S. Sherwin, Generalized thick strip modelling for vortex-induced vibration of long flexible cylinders, Journal of Computational Physics, 321 (2016) 1079-1097.
[34] Y. Bao, H. Zhu, P. Huan, R. Wang, D. Zhou, Z. Han, R. Palacios, M. Graham, S. Sherwin, Numerical prediction of vortex-induced vibration of flexible riser with thick strip method, Journal of Fluids and Structures, 89 (2019) 166-173.
[35] X. Huang, L. He, D.L. Bell, Experimental and computational study of oscillating turbine cascade and influence of part-span shrouds, Journal of fluids engineering, 131 (2009).
[36] D. Serson, J. Meneghini, Numerical study of wings with wavy leading and trailing edges, Imperial College London, 2016.
[37] S. Dong, G.E. Karniadakis, C. Chryssostomidis, A robust and accurate outflow boundary condition for incompressible flow simulations on severely-truncated unbounded domains, Journal of Computational Physics, 261 (2014) 83-105.
[38] C.D. Cantwell, D. Moxey, A. Comerford, A. Bolis, G. Rocco, G. Mengaldo, D. De Grazia, S. Yakovlev, J.-E. Lombard, D. Ekelschot, Nektar++: An open-source spectral/hp element framework, Computer physics communications, 192 (2015) 205-219.
[39] D. Moxey, C.D. Cantwell, Y. Bao, A. Cassinelli, G. Castiglioni, S. Chun, E. Juda, E. Kazemi, K. Lackhove, J. Marcon, Nektar++: Enhancing the capability and application of high-fidelity spectral/hp element methods, Computer Physics Communications, 249 (2020) 107110.
[40] M.E. Nakhchi, S.W. Naung, M. Rahmati, DNS of secondary flows over oscillating low-pressure turbine using spectral/hp element method, International Journal of Heat and Fluid Flow, 86 (2020) 108684.
[41] G.E. Karniadakis, M. Israeli, S.A. Orszag, High-order splitting methods for the incompressible Navier-Stokes equations, Journal of computational physics, 97 (1991) 414-443.
[42] J.-L. Guermond, J. Shen, Velocity-correction projection methods for incompressible flows, SIAM Journal on Numerical Analysis, 41 (2003) 112-134.
[43] M. Rahmati, L. He, D. Wang, Y. Li, R. Wells, S. Krishnababu, Nonlinear time and frequency domain methods for multirow aeromechanical analysis, Journal of Turbomachinery, 136 (2014).
[44] X. Huang, Three-dimensional unsteady flow in the oscillating turbine blade row, Durham University, 2006.
[45] P. Welch, The use of fast Fourier transform for the estimation of power spectra: a method based on time averaging over short, modified periodograms, IEEE Transactions on audio and electroacoustics, 15 (1967) 70-73.
[46] M.A. Alhawwary, Z.J. Wang, DNS and LES of the flow over the T106C turbine using the high-order FR/CPR method, AIAA Scitech 2020 Forum, 2020, pp. 1572.